Frontiers of Physics
https://doi.org/10.1007/s11467-019-0899-y
Front. Phys.
14(5), 53603 (2019)

RESEARCH ARTICLE

High-order exceptional points in non-Hermitian Moiré lattices

Yan-Rong Zhang[1], **Ze-Zheng Zhang**[1], **Jia-Qi Yuan**[1], **Ming Kang**[2,†], **Jing Chen**[1,3,‡]

[1] *MOE Key Laboratory of Weak-Light Nonlinear Photonics, School of Physics, Nankai University, Tianjin 300071, China*
[2] *College of Physics and Materials Science, Tianjin Normal University, Tianjin 300387, China*
[3] *Collaborative Innovation Center of Extreme Optics, Shanxi University, Taiyuan 030006, China*
Corresponding authors. E-mail: †mingkang@mail.nankai.edu.cn, ‡jchen4@nankai.edu.cn
Received January 11, 2019; accepted February 28, 2019

This study proposes an approach to generate high-order exceptional points (EPs) in non-Hermitian systems. A system comprising a homogenous waveguide is considered wherein the imaginary part of the refractive index is modulated using a one-dimensional Moiré profile. This gain-loss modulation couples different lossless waveguide modes, and these hybrid modes can be modeled using a non-Hermitian matrix with complex off-diagonal elements. Results indicate that third-order EPs can be produced by the coalescence of two second-order EPs. Then, the necessary requirements are analyzed using coupled-wave equations and the physical effects of the singularities are discussed.

Keywords exceptional points, non-Hermitian quantum physics, quantum optics, phase transitions

1 Introduction

The concept of exceptional points (EPs) has recently attracted considerable attention in fields of optics and physics. Originating from a purely mathematical context, EPs represent branch point singularities in the spectra of parameter-dependent linear operators [1]. Heiss and Harney [2] showed that an EP in the wave function of a Hamiltonian is a specific superposition of two configurations when the wave function involves a complex interaction parameter. Similar to phase transition points in non-Hermitian systems, the sharp features observed around EPs cause many intriguing phenomena in various systems, such as optical microcavities, coupled atom–cavity systems, photonic crystals, exciton–polariton billiards, parity–time ($\mathcal{PT}$)-symmetric systems, and acoustic systems [3–21]. The unique properties of EPs, such as the topologies of the self-intersecting Riemann sheets around them, have been extensively studied. Further, various practical applications that employ EPs, such as loss-induced transmission, unidirectional invisibility, laser mode selection, enhanced sensors, topological energy transfer, and slow light have been proposed [10, 11, 18, 22–28].

Although EPs were originally proposed for two-level quantum systems, they can be generalized to N-level systems to realize high-order EPs [28–38]. High-order EPs are singularities in the parameter spaces of physical systems containing $N > 2$ constituent modes, wherein the corresponding eigenvectors become equal [29]. Using high-order EPs to further amplify the effect of perturbations for achieving even greater sensitivity has gained particular research interest [28, 31]. The possibility of enhanced spontaneous emissions at high-order EPs has also been studied [32].

Owing to many attractive characteristics of EPs, versatile methods for generating EPs with arbitrary orders must be identified. The most common approach is to initially use identical resonators, such as parallel waveguides or ring cavities, and then introduce distributed gain–loss perturbations via $\mathcal{PT}$ symmetry [15, 22, 23, 27, 28]. By treating the gains and losses as perturbations of the complex resonant frequencies, wave dynamics of coupled systems can mathematically described in terms of non-Hermitian matrices with complex diagonal elements. Simple linear algebra methods can then reveal the primary characteristics of EPs that separate broken and conserved $\mathcal{PT}$ phases. This approach forms the basis of a wide range of studies from phase breaking in complex optical potentials [23] to enhancing sensitivity in coupled cavities [28] and slow light [27].

This study proposes an approach to realize high-order EPs. Mathematically, the diagonal elements in this approach are real, but the complex off-diagonal elements are not conjugates of each other. The off-diagonal elements represent the interactions between different guided modes; therefore, this approach can be applied to any non-Hermitian waveguide structure with a suitable grating in the complex dielectric constant. $\mathcal{PT}$-symmetric optical lattices employ a similar approach to manipulate the beam dynamics [39] in single-waveguide structures to realize unidirectional invisibility [25] and in surface gratings to generate unidirectional, long-lifetime surface waves [26]. A high-order EP requires coupling among $N > 2$ modes; therefore, the proposed approach utilizes the concept of

© Higher Education Press and Springer-Verlag GmbH Germany, part of Springer Nature 2019

Moiré optical lattices [40, 41] formed by the beating frequency between two Bragg gratings with similar periods. Beam dynamics in non-Hermitian Moiré lattices is studied, and the merging of two initially second-order EPs (EP2s) to form a third-order EP (EP3) with increasing modulation strength is investigated. This study highlights the importance of Moiré lattices and paves way for generating, manipulating, and utilizing non-Hermitian degeneracies in various fields, including photonics, optomechanics, and microwave and atomic physics.

2 Theory

This study investigates a system comprising a homogenous waveguide structure with a one-dimensional perturbation in the dielectric constant ε in the x direction, as shown in Fig. 1. The incident plane wave is polarized in the z direction, and the wavevector lies in the x–y plane. However, unlike conventional Moiré gratings, we assume that the modulation is imposed on the imaginary component of ε as follows:

$$\varepsilon(x) = \varepsilon_w + j\frac{\delta\varepsilon}{2}[\cos(g_1 x) + \cos(g_2 x)], \tag{1}$$

where

$$g_{1,2} = g \pm G, \tag{2}$$

where g and G are the Bragg and Moiré spatial frequencies, respectively, and $g \gg G$. The perturbation is very weak with respect to the real part of the background ε_w, i.e., $\delta\varepsilon \ll \varepsilon_w$.

The effect of this perturbation on the propagation of optical field can be analyzed by solving Maxwell's equations [40]. Considering a mode propagating in the x–y plane and assuming its electric component is $\boldsymbol{E} = E_z \exp(-\mathrm{i}k_y y - \mathrm{i}\beta x + \mathrm{i}\omega t)\hat{z}$ without loss of generality, the dispersion can be represented as follows:

$$\frac{1}{\varepsilon(x)}\nabla \times \nabla \times \boldsymbol{E} = \frac{\omega^2}{c^2}\boldsymbol{E}. \tag{3}$$

Based on Bloch theory and by considering the two harmonic contributions to $\mathrm{Im}\{\varepsilon\}$, we see that $\boldsymbol{E}$ is a superposition of several different plane waves:

$$\boldsymbol{E} = \hat{z}\exp(-\mathrm{i}k_y y + \mathrm{i}\omega t)\sum_{n,m} A_{n,m}\exp(-\mathrm{i}\beta_{n,m}x). \tag{4}$$

Here, the wavevectors are defined as

$$\beta_{n,m} = \beta + ng_1 + mg_2, \tag{5}$$

where n and m are integers.

Substituting Eqs. (4) and (1) into Eq. (3) and using the following approximation,

$$\frac{1}{\varepsilon(x)} = \frac{1}{\varepsilon_w} - j\frac{\delta\epsilon}{2\varepsilon_w^2}[\cos(g_1 x) + \cos(g_2 x)], \tag{6}$$

we can obtain the full-matrix formula as follows:

$$\sum_{n,m} M_{n,m}^{n',m'}(\beta_{n,m}^2 + k_y^2)A_{n,m} = \varepsilon_w\frac{\omega^2}{c^2}A_{n',m'}. \tag{7}$$

Let $\Delta = \delta\epsilon/(4\varepsilon_w)$; then,

$$M_{n,m}^{n',m'} = \delta_{n,n'}\delta_{m,m'} - j\Delta(\delta_{n,n'\pm1}\delta_{m,m'} + \delta_{n,n'}\delta_{m,m'\pm1}). \tag{8}$$

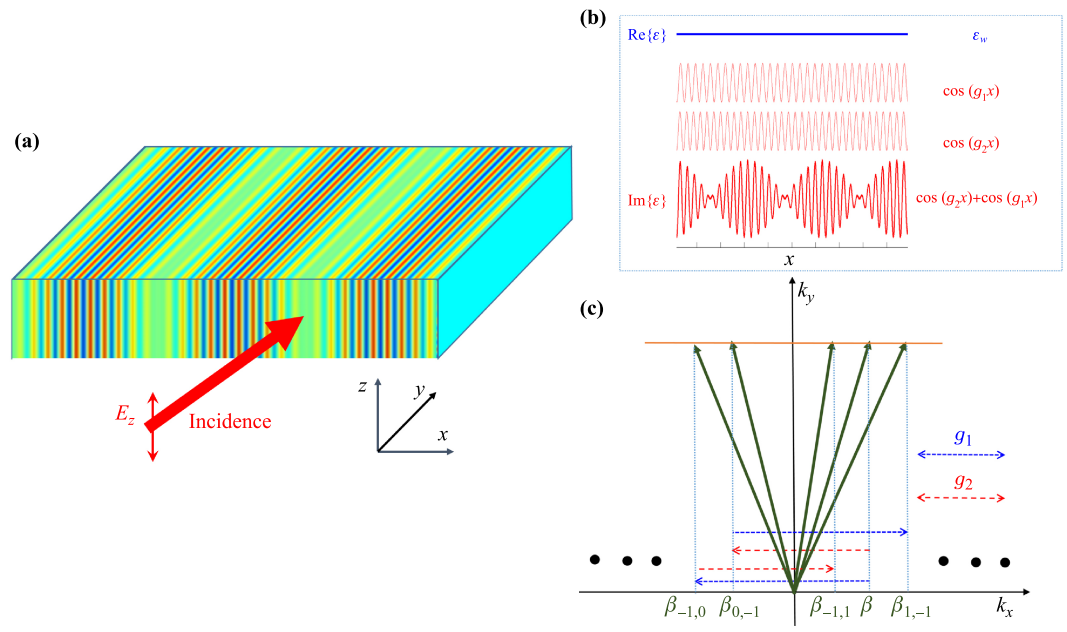

Fig. 1 Schematic of **(a)** a non-Hermitian Moiré lattice with **(b)** a dielectric constant perturbation of $\mathrm{Im}\{\varepsilon\} \propto \cos(g_1 x) + \cos(g_2 x)$. The real part ε_R of ε is constant. **(c)** Illustration of the phase-matching conditions $\beta_{n,m} = \beta + ng_1 + mg_2$.

Here, $\delta_{i,j}$ is the Kronecker delta function. The matrix $\boldsymbol{M}$ that determines the eigenfrequencies and eigenfunctions of the coupled modes is clearly non-Hermitian because the off-diagonal elements are complex but not conjugates of each other, i.e., $M_{n,m} \neq M^*_{m,n}$. Thus, the dispersion curves may show EPs.

In general, Eq. (7) represents the coupling between infinite modes that are mediated by the perturbation shown in Eq. (1). This study focuses on the modes at the Brillouin zone (BZ) edge $\beta \sim g/2$ in the Moiré lattice; therefore, only the components with almost degenerate energies is retained. This reduces the full matrix to the 3×3 matrix

$$\begin{pmatrix} m_{11} & -j\Delta m_{22} & 0 \\ -j\Delta m_{11} & m_{22} & -j\Delta m_{33} \\ 0 & -j\Delta m_{22} & m_{33} \end{pmatrix} \begin{pmatrix} A_{-1,0} \\ A_{0,0} \\ A_{0,-1} \end{pmatrix} = \varepsilon_w \frac{\omega^2}{c^2} \begin{pmatrix} A_{-1,0} \\ A_{0,0} \\ A_{0,-1} \end{pmatrix}, \tag{9}$$

where

$$m_{11} = (\beta - g_1)^2 + k_y^2, \tag{10a}$$
$$m_{22} = \beta^2 + k_y^2, \tag{10b}$$
$$m_{33} = (\beta - g_2)^2 + k_y^2. \tag{10c}$$

Equation (9) provides a good approximation of the dispersion at the BZ edge $g/2$. Figure 2 shows some results obtained by comparing strict calculations using the full-matrix formula in Eq. (7) (blue dots) with the results obtained from the reduced 3×3 matrix in Eq. (9) (red lines). Both results agree well with each other. For simplicity, the reduced 3×3 matrix is used for calculation and analysis.

3 Simulation and analysis

3.1 Spontaneous emergence of EP2s

We analyze the dispersion and field distributions of these non-Hermitian Moiré lattices. Figure 3 shows the results for two example cases, $\delta\varepsilon = 0.0002$ and 0.0006, using $k_y = 10g$, $G = 0.01g$, and $\varepsilon_w = 4$.

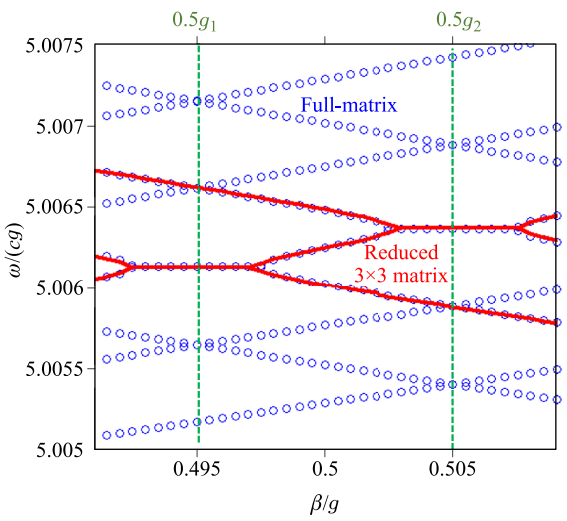

Fig. 2 Dispersion curves for the full-matrix (blue dots) and reduced 3×3 matrix (red lines) methods when $G = 0.01g$, $\varepsilon_w = 4$, and $\delta\varepsilon = 0.0006$.

These results indicate that EPs are observed in the dispersion curves even for very weak perturbations $\delta\varepsilon$. Four, two, and two EPs exist near the BZ edge, around the wavevector $g_1/2$, and near $g_2/2$, respectively (Fig. 3). A broken $\mathcal{PT}$ phase is observed between each pair of EPs. Figure 3(b) shows that in these broken $\mathcal{PT}$-phase regions, the degenerate real parts of the eigenfrequencies ($\mathrm{Re}\{\omega\}$) are associated with opposite imaginary parts ($\mathrm{Im}\{\omega\}$). This association creates circles in the two-dimensional space formed by the wavevectors β and $\mathrm{Im}\{\omega\}$.

The formation of these EPs is thresholdless. In other words, even with infinitely small Δ values, the $\mathcal{PT}$ phase is broken and the eigenfrequencies ω are complex. To deduce

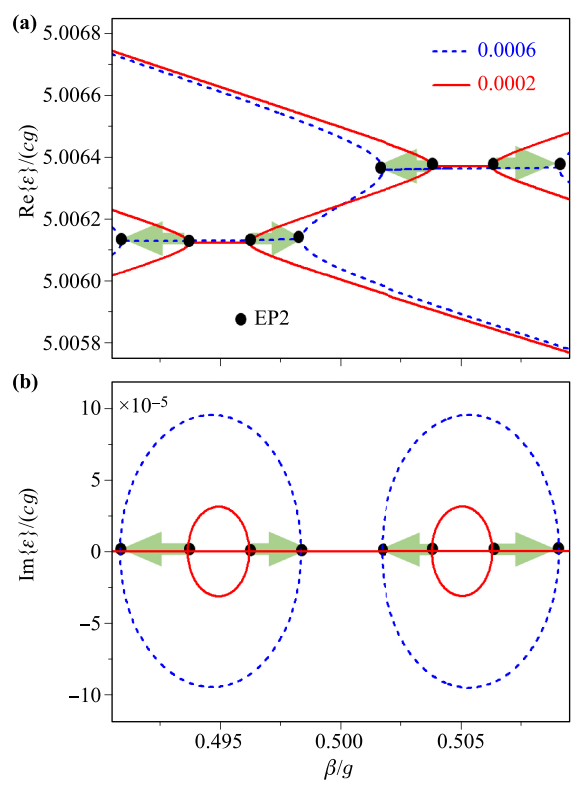

Fig. 3 **(a)** Real and **(b)** imaginary parts of the eigenfrequencies ω for $\delta\varepsilon$ values of 0.0002 (red solid lines) and 0.0006 (blue dashed lines). The other parameters are $k_y = 10g$, $G = 0.01g$, and $\varepsilon_w = 4$.

the cause of such a formation, we focus on the wavevector for $\beta = g_1/2$ and assume $\Delta \ll 1$. The $\mathrm{Im}\{\omega\}$ ring shown in Fig. 3(b) is small, and the upper dispersion curve of $\omega^2 = [k_y^2 + (\beta - g_2)^2]/\varepsilon_w$ is separated from the two degenerate curves of $\omega^2 = (k_y^2 + \beta^2)/\varepsilon_w$ and $\omega^2 = [k_y^2 + (\beta - g_1)^2]/\varepsilon_w$. In this case, the $\mathcal{PT}$ phase can be approximated using the 2×2 matrix

$$\omega_0^2 \begin{pmatrix} 1 & -j\Delta \\ -j\Delta & 1 \end{pmatrix} \begin{pmatrix} A_{-1,0} \\ A_{0,0} \end{pmatrix} = \varepsilon_w \omega^2 \begin{pmatrix} A_{-1,0} \\ A_{0,0} \end{pmatrix}, \quad (11)$$

where $\omega_0^2 = (g_1^2/4 + k_y^2)c^2$. The eigenfrequencies, $\omega_\pm = \omega_0\sqrt{\varepsilon_w(1 \pm j\Delta)} \sim \omega_0\sqrt{\varepsilon_w}(1 \pm j\Delta/2)$, are complex and conjugates of each other as long as $\Delta \neq 0$. $\beta = g_2/2$ can be analyzed in a similar manner.

The eigenfunctions and field distributions are determined to prove that the degenerate points are EPs. Figure 4 shows the so-called c-product $\langle \Psi^* | \Psi \rangle = A_{-1,0}^2 + A_{0,0}^2 + A_{0,-1}^2$ for the eigenfunction $\Psi^{\mathrm{T}} = [A_{-1,0}, A_{0,0}, A_{0,-1}]^{\mathrm{T}}$. Usually, c-product value is approximately 1, but it sharply decreases near EPs, approaching zero. This phenomenon signifies the unique chirality, i.e., self-orthogonality, of EPs [2, 27–30, 42, 43]. Herein, c-product is identical to the phase rigidity utilized in a previous study [30, 44] because our calculations require the inner product $\langle \Psi | \Psi \rangle = |A_{-1,0}|^2 + |A_{0,0}|^2 + |A_{0,-1}|^2 = 1$.

Figure 5 shows the field distributions at two selected dispersion points when $\delta\varepsilon = 0.0006$ and $k = 0.49834g$ (refer to the inset). The eigenfunction Ψ^T at the lower degenerate point (EP2) is $[0.068 + 0.685\mathrm{i}, -0.707, 0.004 - 0.164\mathrm{i}]^{\mathrm{T}}$, which is self-orthogonal, i.e., the c-product $\langle \Psi^* | \Psi \rangle$ is zero. The main component of the eigenfunction is the chiral component $[A_{-1,0}, A_{0,0}]^{\mathrm{T}} = [\mathrm{i}, -1]^{\mathrm{T}}/\sqrt{2}$, which is the eigenfunction of an EP2 in a two-level system [2, 27, 29, 30]. This also validates the approximation used in Eq. (11) when the thresholdless nature of EPs are discussed. Interference between the two components k and $k - g_1$ produces the strong oscillating pattern shown in Fig. 5(b), where the field can reach zero. For comparison, the eigenfunction at the upper dispersion point A is $[-0.055, -0.275\mathrm{i}, 0.960]^{\mathrm{T}}$. Herein, the main component is the mode with wavevector $k - g_2$. Thus, the field distribution [Fig. 5(a)] is nearly homogenous, with only a very weak oscillating modulation.

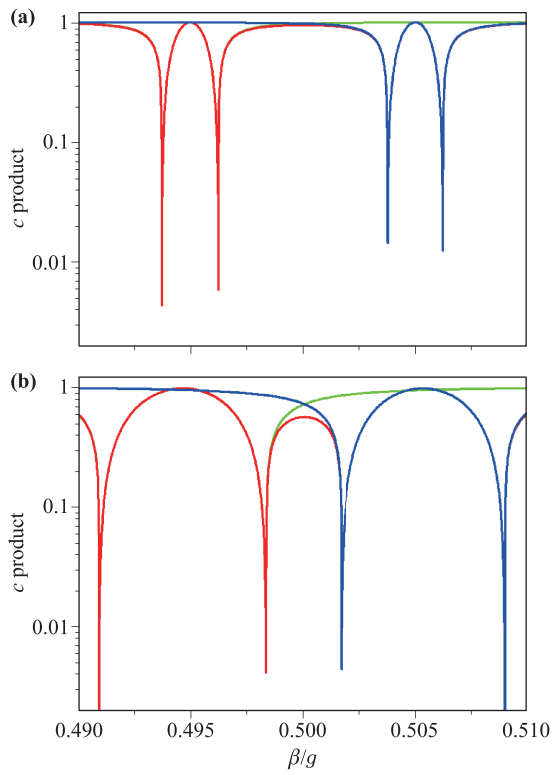

Fig. 4 Variations in the c-products of all the eigenfunctions for $\delta\varepsilon$ values of **(a)** 0.0002 and **(b)** 0.0006. At EPs, the c-product approaches zero.

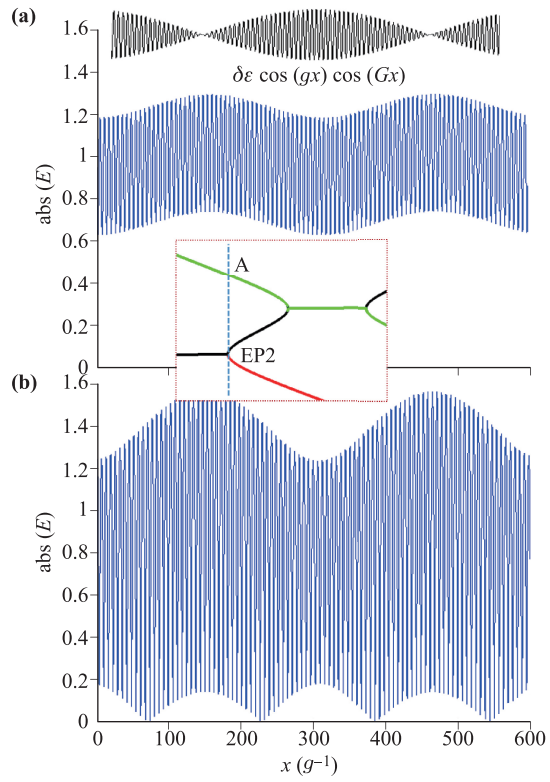

Fig. 5 Eigenmode distributions for the **(a)** upper dispersion point A and **(b)** lower degeneracy point EP2 [refer to the inset] when $\delta\varepsilon = 0.0006$ and $\beta = 0.49834g$. To determine the relative distribution of field with respect to the Moiré lattice, the pattern of $\mathrm{Im}\{\varepsilon\}$ is shown at the top of the figure.

3.2 From EP2s to an EP3

The aforementioned analysis reveals that EPs are generated in non-Hermitian Moiré lattices even for very small perturbations $\delta\varepsilon$. These degenerate points are generally EP2s, and the associated wavevectors β can be manipulated by changing $\delta\varepsilon$. The two central EP2s move toward each other as $\delta\varepsilon$ increases; therefore, they may create an

EP3 by merging together via an EP2+EP2=EP3 process, as indicated by the arrows in Figs. 3, 4, and 6.

To predict the conditions required to create an EP3, we can assume that EP3 occurs near $\beta = g/2$. Given that $G \ll g \ll k_y$, we can also assume the approximations $m_{11} = m_{22} + gG$ and $m_{33} = m_{22} - gG$. Substituting these values into Eq. (9), ignoring high-order perturbation terms, such as ΔgG, and requiring that the three solutions are identical, we obtain

$$\delta\varepsilon_{EP3} = 2\sqrt{2}\frac{gG\varepsilon_w}{k_y^2 + g^2/4} \tag{12}$$

when $\omega_{EP3} = c(k_y^2+g^2/4)^{0.5}\varepsilon_w^{-0.5}$. Considering the parameters utilized in our simulations, the critical value $\delta\varepsilon_{EP3}$ required to produce an EP3 is predicted to be 1.13×10^{-3}.

Indeed, our calculations indicate that an EP3 is formed by the coalescence of two EP2s when $\delta\varepsilon = 1.11\times10^{-3}$, as shown in Fig. 6. Three dispersion curves are observed, of which two have the same real eigenfrequencies. These doubly-Re$\{\omega\}$-degenerate solutions are the lower (upper) curves before (after) $g/2$; due to their opposite imaginary components, they form the half rings observed in Fig. 6(b). The other dispersion curve has a zero Im$\{\omega\}$ value. EP3 occurs at $\beta \sim g/2$. After determining the eigenfunctions, we can confirm that the three solutions coalesce into one

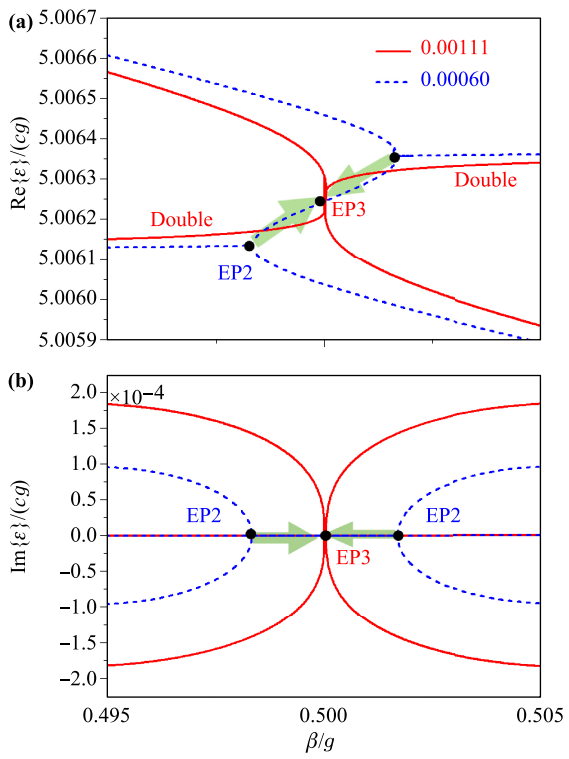

Fig. 6 Dispersions of the **(a)** real and **(b)** imaginary components of the eigenfrequencies at EP3. Arrows indicate the occurrence of EP2+EP2=EP3 process as $\delta\varepsilon$ increases. The lower (upper) curves before (after) $g/2$ doubly degenerate in Re$\{\omega\}$ and have opposite nonzero Im$\{\omega\}$ values.

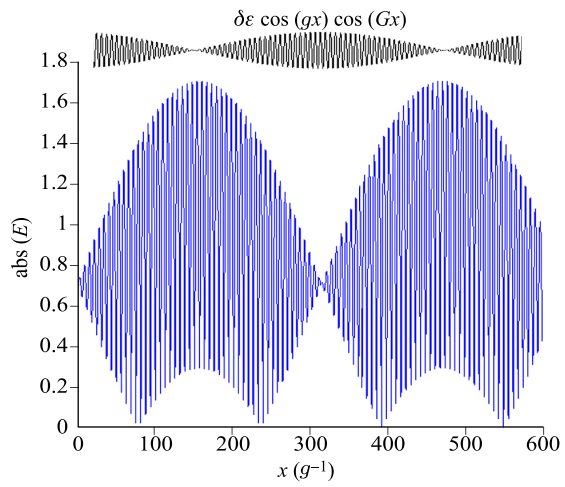

Fig. 7 Field amplitude distributions at EP3.

solution as follows:

$$\Psi_{EP3} = \frac{1}{2}\begin{pmatrix} 1 \\ \mathrm{i}\sqrt{2} \\ -1 \end{pmatrix}. \tag{13}$$

Equation (13) is just a standard type of EP eigenfunction [36] with a zero c-product.

Figure 7 shows the field distribution at EP3, which is substantially different from that for EP2 shown in Fig. 5(b). In the regions of maximum Im$\{\varepsilon\}$, the field amplitude oscillations are quenched and approach zero. This phenomenon is closely related to the unique eigenfunction of EP3; according to Eq. (13), the $\beta - g_1$ and $\beta - g_2$ components have equal weights, i.e., $A_{-1,0} = -A_{0,-1}$. Interference between them produces spatially periodic patterns with a super period identical to that of $\cos(gx)\cos(Gx)$. Unlike scenarios wherein nodes with zero field amplitude can be obtained with classic Moiré gratings [40, 41], a phase difference of $\pi/2$ ($-\pi/2$) is observed between $\beta - g_1$ ($\beta - g_2$) and β components. Consequently, the homogenous background field associated with the β component is not modified.

4 Discussion

We proved that EP3s can be found in non-Hermitian Moiré lattices. The current interest in EPs is not only owing to their great academic importance but also because they have a wide variety of potential applications in different fields. The proposed approach can be experimentally validated. Further, methods of manipulating the imaginary component of ε or equivalently the loss and gain coefficients have been previously proposed [25, 42, 43]. Experimental techniques utilizing photonic lattices [13, 39, 41] also have great potential. However, in realistic situations, the modulation coefficient $\delta\varepsilon$ is generally very weak although Eq. (12) implies that sufficiently large k_y values

could enable us to circumvent such limitations on large $\delta\varepsilon$ values. This is also a significant advantage of photonic lattices [13, 39, 41].

This study focuses on discussing the transverse electrical mode in Moiré lattices; a similar analysis can also be applied to the transverse magnetic mode [45]. In addition, the dielectric constant ε_w is generally real; however, in passive scenarios with a residual absorption background, ε_w can become complex. However, this does not change the physics discussed herein.

Potential applications of the effect presented herein could also be utilized to enhance sensitivity [28] and spontaneous emissions [32] as well as other nonlinear effects via the slow-light effect of EPs [27]. Realizing high-order EPNs ($N > 3$) in quasi-periodic or even disordered systems via an approach that is similar to the proposed approach is essential. The possible physical mechanisms involved and applications of these ideas require further discussion.

5 Conclusion

In summary, EP3s can be produced in non-Hermitian Moiré lattices by the coalescence of two EP2s via the EP2+EP2=EP3 process. The necessary requirements are analyzed using coupled-wave equations, and the physical effects of EP3s are discussed. The proposed approach could also be extended to structures with more harmonic expansion terms, such as quasi-periodic super-lattices. This study highlights the importance of Moiré lattices and paves the way toward generating, manipulating, and utilizing high-order EPs in various fields.

Acknowledgements Y. R. Z., Z. Z. Z., and J. Q. Y. contributed equally to this study. The authors acknowledge support from the National Natural Science Foundation of China (NSFC) under Grant Nos. 11574162, 11674244, and 11874228.

References

1. T. Kato, Perturbation Theory of Linear Operators, Berlin: Springer-Verlag Berlin Heidelberg, 1966
2. W. D. Heiss and H. L. Harney, The chirality of exceptional points, *Eur. Phys. J. D* 17(2), 149 (2001)
3. C. Dembowski, B. Dietz, H. D. Graf, H. L. Harney, A. Heine, W. D. Heiss, and A. Richter, Observation of a chiral state in a microwave cavity, *Phys. Rev. Lett.* 90(3), 034101 (2003)
4. J. Wiersig, Formation of long-lived, scarlike modes near avoided resonance crossings in optical microcavities, *Phys. Rev. Lett.* 97(25), 253901 (2006)
5. B. Dietz, T. Friedrich, J. Metz, M. Miski-Oglu, A. Richter, F. Schafer, and C. A. Stafford, Rabi oscillations at exceptional points in microwave billiards, *Phys. Rev. E* 75(2), 027201 (2007)
6. S. B. Lee, J. Yang, S. Moon, S. Y. Lee, J. B. Shim, S. W. Kim, J. H. Lee, and K. An, Observation of an exceptional point in a chaotic optical microcavity, *Phys. Rev. Lett.* 103(13), 134101 (2009)
7. Q. H. Song and H. Cao, Improving optical confinement in nanostructures via external mode coupling, *Phys. Rev. Lett.* 105(5), 053902 (2010)
8. S. Bittner, B. Dietz, U. Gunther, H. L. Harney, M. Miski-Oglu, A. Richter, and F. Schafer, $\mathcal{PT}$ symmetry and spontaneous symmetry breaking in a microwave billiard, *Phys. Rev. Lett.* 108(2), 024101 (2012)
9. M. Liertzer, L. Ge, A. Cerjan, A. D. Stone, H. E. Tureci, and S. Rotter, Pump-induced exceptional points in lasers, *Phys. Rev. Lett.* 108(17), 173901 (2012)
10. X. Yin and X. Zhang, Unidirectional light propagation at exceptional points, *Nat. Mater.* 12(3), 175 (2013)
11. M. Brandstetter, M. Liertzer, C. Deutsch, P. Klang, J. Schoberl, H. E. Tureci, G. Strasser, K. Unterrainer, and S. Rotter, Reversing the pump dependence of a laser at an exceptional point, *Nat. Commun.* 5(1), 4034 (2014)
12. M. Kang, H. X. Cui, T. F. Li, J. Chen, W. Zhu, and M. Premaratne, Unidirectional phase singularity in ultrathin metamaterials at exceptional points, *Phys. Rev. A* 89(6), 065801 (2014)
13. S. Longhi and G. Della Valle, Optical lattices with exceptional points in the continuum, *Phys. Rev. A* 89(5), 052132 (2014)
14. H. Cao and J. Wiersig, Dielectric microcavities: Model systems for wave chaos and non-Hermitian physics, *Rev. Mod. Phys.* 87(1), 61 (2015)
15. H. Hodaei, M. A. Miri, A. U. Hassan, W. E. Hayenga, M. Heinrich, D. N. Christodoulides, and M. Khajavikhan, Parity–time-symmetric coupled microring lasers operating around an exceptional point, *Opt. Lett.* 40(21), 4955 (2015)
16. B. Zhen, C. W. Hsu, Y. Igarashi, L. Lu, I. Kaminer, A. Pick, S. Chua, J. D. Joannopoulos, and M. Soljacic, Spawning rings of exceptional points out of Dirac cones, *Nature* 525(7569), 354 (2015)
17. A. Cerjan, A. Raman, and S. Fan, Exceptional contours and band structure design in parity–time symmetric photonic crystals, *Phys. Rev. Lett.* 116(20), 203902 (2016)
18. J. Doppler, A. A. Mailybaev, J. Böhm, U. Kuhl, A. Girschik, F. Libisch, T. J. Milburn, P. Rabl, N. Moiseyev, and S. Rotter, Dynamically encircling an exceptional point for asymmetric mode switching, *Nature* 537(7618), 76 (2016)
19. L. Ge, Anomalous parity–time-symmetry transition away from an exceptional point, *Phys. Rev. A* 94(1), 013837 (2016)
20. M. Kang, J. Chen, and Y. D. Chong, Chiral exceptional points in metasurfaces, *Phys. Rev. A* 94(3), 033834 (2016)
21. K. H. Kim, M. S. Hwang, H. R. Kim, J. H. Choi, Y. S. No, and H. G. Park, Direct observation of exceptional points in coupled photonic-crystal lasers with asymmetric optical gains, *Nat. Commun.* 7(1), 13893 (2016)

22. M. Lawrence, N. Xu, X. Zhang, L. Cong, J. Han, W. Zhang, and S. Zhang, Manifestation of $\mathcal{PT}$ symmetry breaking in polarization space with terahertz metasurfaces, *Phys. Rev. Lett.* 113(9), 093901 (2014)
23. A. Guo, G. J. Salamo, D. Duchesne, R. Morandotti, M. Volatier-Ravat, V. Aimez, G. A. Siviloglou, and D. N. Christodoulides, Observation of PT-symmetry breaking in complex optical potentials, *Phys. Rev. Lett.* 103(9), 093902 (2009)
24. S. Longhi, $\mathcal{PT}$-symmetric laser absorber, *Phys. Rev. A* 82(3), 031801 (2010) (R)
25. L. Feng, Y. L. Xu, W. S. Fegadolli, M. H. Lu, J. E. B. Oliveira, V. R. Almeida, Y. F. Chen, and A. Scherer, Experimental demonstration of a unidirectional reflectionless parity–time metamaterial at optical frequencies, *Nat. Mater.* 12(2), 108 (2013)
26. W. Wang, L. Q. Wang, R. D. Xue, H. L. Chen, R. P. Guo, Y. Liu, and J. Chen, Unidirectional excitation of radiative-loss-free surface plasmon polaritons in $\mathcal{PT}$-symmetric systems, *Phys. Rev. Lett.* 119(7), 077401 (2017)
27. T. Goldzak, A. A. Mailybaev, and N. Moiseyev, Light stops at exceptional points, *Phys. Rev. Lett.* 120(1), 013901 (2018)
28. H. Hodaei, A. U. Hassan, S. Wittek, H. Garcia-Gracia, R. El-Ganainy, D. N. Christodoulides, and M. Khajavikhan, Enhanced sensitivity at higher-order exceptional points, *Nature* 548(7666), 187 (2017)
29. W. D. Heiss, Chirality of wavefunctions for three coalescing levels, *J. Phys. A* 41(24), 244010 (2008)
30. K. Ding, Z. Q. Zhang, and C. T. Chan, Coalescence of exceptional points and phase diagrams for one-dimensional $\mathcal{PT}$-symmetric photonic crystals, *Phys. Rev. B* 92(23), 235310 (2015)
31. W. D. Heiss and G. Wunner, Resonance scattering at third-order exceptional points, *J. Phys. A* 48(34), 345203 (2015)
32. Z. Lin, A. Pick, M. Loncar, and A. W. Rodriguez, Enhanced spontaneous emission at third-order Dirac exceptional points in inverse-designed photonic crystals, *Phys. Rev. Lett.* 117(10), 107402 (2016)
33. H. Jing, K. Ozdemir, H. Lu, and F. Nori, High-order exceptional points in optomechanics, *Sci. Rep.* 7(1), 3386 (2017)
34. M. Y. Nada, M. A. K. Othman, and F. Capolino, Theory of coupled resonator optical waveguides exhibiting high-order exceptional points of degeneracy, *Phys. Rev. B* 96(18), 184304 (2017)
35. J. Schnabel, H. Cartarius, J. Main, G. Wunner, and W. D. Heiss, $\mathcal{PT}$-symmetric waveguide system with evidence of a third-order exceptional point, *Phys. Rev. A* 95(5), 053868 (2017)
36. J. Kullig, C. H. Yi, M. Hentschel, and J. Wiersig, Exceptional points of third-order in a layered optical microdisk cavity, *New J. Phys.* 20(8), 083016 (2018)
37. Q. Zhong, D. N. Christodoulides, M. Khajavikhan, K. G. Makris, and R. El-Ganainy, Power-law scaling of extreme dynamics near higher-order exceptional points, *Phys. Rev. A* 97(2), 020105 (2018) (R)
38. X. Zhou, S. K. Gupta, Z. Huang, Z. Yan, P. Zhan, Z. Chen, M. Lu, and Z. Wang, Optical lattices with higher-order exceptional points by non-Hermitian coupling, *Appl. Phys. Lett.* 113(10), 101108 (2018)
39. K. G. Makris, R. El-Ganainy, D. N. Christodoulides, and Z. H. Musslimani, Beam dynamics in $\mathcal{PT}$ symmetric optical lattices, *Phys. Rev. Lett.* 100(10), 103904 (2008)
40. J. B. Khurgin, Light slowing down in Moiré fiber gratings and its implications for nonlinear optics, *Phys. Rev. A* 62(1), 013821 (2000)
41. R. D. Xue, W. Wang, L. Q. Wang, H. L. Chen, R. P. Guo, and J. Chen, Localization and oscillation of optical beams in Moiré lattices, *Opt. Express* 25(5), 5788 (2017)
42. L. Feng, R. El-Ganainy, and L. Ge, Non-Hermitian photonics based on parity–time symmetry, *Nat. Photonics* 11(12), 752 (2017)
43. R. El-Ganainy, K. G. Makris, M. Khajavikhan, Z. H. Musslimani, S. Rotter, and D. N. Christodoulides, Non-Hermitian physics and $\mathcal{PT}$ symmetry, *Nat. Phys.* 14(1), 11 (2018)
44. I. Rotter, A non-Hermitian Hamilton operator and the physics of open quantum systems, *J. Phys. A* 42(15), 153001 (2009)
45. W. Zhang, A. Hu, X. Lei, N. Xu, and N. Ming, Photonic band structures of a two-dimensional ionic dielectric medium, *Phys. Rev. B* 54(15), 10280 (1996)